

Design of a Plasmonic Absorption Electro-optical Modulator Based on n-doped Silicon and Barium Titanate

Purya Es'haghi^{a*}, Ali Barkhordari^b and Abolfazl Safaei Bezgabadi^a

^a*Photonics Department, Graduate University of Advanced Technology, Kerman, Iran;*

^b*Department of plasma engineering, Graduate University of Advanced Technology, Kerman, Iran*

*Corresponding Author: puryae@gmail.com

Abstract:

In this paper, a numerical solution for a plasmonic absorption modulator with a six-layer structure consisting of an air superstrate, a gold layer, a barium titanate layer, a n type silicon layer, a gold layer and a thin-shell nanolattice aluminium oxide substrate is presented. Regarding the suggested structure, parameters related to the absorption modulation are investigated at different thicknesses. Here, the Pockels effect and the free carrier dispersion effect are considered simultaneously. The dispersion relation of this structure is analytically obtained and numerically solved by the Nelder-Mead method. The maximum calculated figure of merit is 12.79. Furthermore, according to our results, it is understood that this modulator has a high ability to be utilized in optical communication systems. Also, it could be integrated to the microelectronic systems and it is compatible with CMOS technology.

Keywords: Plasmonic modulator; Nelder-Mead method; Pockels effect; Free carrier dispersion effect; Optical communication.

1. Introduction

According to Moore's law, the number of transistors in a fixed area of dense integrated circuit doubles almost every two years and consequently electronic devices are going to be more compact. Because of the diffraction limit, optical waveguides do not have compaction capability below the half of propagation wavelength. Hence, they can't be integrated with electronic devices. This is a defect in waveguide-based systems. Recently, scientists have turned to plasmonic waveguides in order to overcome the diffraction limit [1-3].

It is important to use the plasmonic waveguide-based modulators and switches. As these modulators and switches have footprints on the order of several μm^2 , they have the capability to cointegrate with electronic systems [4,5]. These types of modulators and switches have many advantages, such as high bandwidth [6], low power consumption [7], and ultra-compact size [8]. Also, these modulators and switches mainly employ the thermal optics effect [9-11], the free carrier dispersion effect [12,13], the Pockels effect [14-16], the phase transition effect [17-19] and the electrochemical metallization effect [20,21]. Owing to the usage of different types of waveguides based on surface plasmon polaritons, these devices have a strong interaction between propagating optical signals and active materials [22-27], which is necessary to produce optical switches well.

As silicon-based Metal-Insulator-Metal waveguides can be created with a volumetric size of a cubic wavelength they are suitable for planar integration. Hence, they are compatible with CMOS technology and are able to integrate with microelectronics devices. The modulators based on these waveguides need a low operation voltage. These offer a large modulation depth and furthermore provide a switching speed as fast as several gigahertz [28].

Here, a silicon-based plasmonic modulator is presented which it has an Air/Au/BaTiO₃/n-Si/Au/thin-shell nanolattice Al₂O₃ configuration. This structure is studied as an intensity modulator at the 1.55μm wavelength. The dispersion relation for this structure is obtained and solved for 0 and 10V applied voltages in order to analyze its properties. Therefore, the Poisson equation is solved to apply an electric field to the voltage-dependent variation of the refractive index. It should be noted that the free carrier dispersion effect and the Pockels effect are simultaneously considered in this device.

2. Theory

2.1. Modulator Structure

As it is understood, the presented structure is a slab waveguide. This waveguide consists of two layers of n-type Silicon and barium titanate which are embedded between two layers of Au. The substrate of this structure is a thin-shell nanolattice aluminium oxide (TSNAO) with near unity refractive index. The above region of the structure is filled with the air. The BaTiO₃ is a birefringent crystal that matches its principal-axis system to the axes of the considered coordinate system. Figure 1 shows the structure of the investigated modulator. The refractive indices of each layer, which form the modulator, can be given by:

$$n_{\text{TSNAO}} = 1.025 \quad (1)$$

$$n_{\text{Au}}^2 = 1.53 - \frac{1}{145^2 \left(\frac{1}{\lambda^2} + \frac{i}{17000\lambda} \right)} + \frac{0.94}{468} \left[\frac{e^{-i\pi/4}}{\left(\frac{1}{468} - \frac{1}{\lambda} - \frac{i}{2300} \right)} + \frac{e^{-i\pi/4}}{\left(\frac{1}{468} + \frac{1}{\lambda} + \frac{i}{2300} \right)} \right] + \frac{1.36}{331} \left[\frac{e^{-i\pi/4}}{\left(\frac{1}{331} - \frac{1}{\lambda} - \frac{i}{940} \right)} + \frac{e^{-i\pi/4}}{\left(\frac{1}{331} + \frac{1}{\lambda} + \frac{i}{940} \right)} \right] \quad (2)$$

$$\epsilon_{\text{n-Si}} = \epsilon_{\infty} - \frac{\omega_p^2}{[\omega^2(1 + \frac{1}{\omega\tau})]}, \quad \omega_p^2 = \frac{N_i e^2}{\epsilon_0 m^*}, \quad \tau = \frac{m^* \mu}{e} \quad (3)$$

where $\mu = 50 \text{ cm}^2/\text{Vs}$, $m_e = 9.1 \times 10^{-31} \text{ kg}$, $m^* = 0.272m_e$, $\epsilon_{\infty} = 11.7$, $e = 1.602 \times 10^{-19} \text{ C}$ and $\epsilon_0 = 8.85 \times 10^{-12} \text{ C}^2/\text{Nm}^2$ for substrate Au layer and n-Si layer, respectively [29-31]. Also, the ordinary and extraordinary refractive indexes of the BaTiO₃ can be written as [32]:

$$n_o^2 = 3.05840 + \frac{2.27326 \lambda^2}{\lambda^2 - 0.07409} - 0.02428 \lambda^2 \quad (4)$$

$$n_e^2 = 3.02479 + \frac{2.14062 \lambda^2}{\lambda^2 - 0.067007} - 0.02169 \lambda^2 \quad (5)$$

In equations (1) to (5), n , λ , ϵ_{∞} , ω_p , τ , μ , m_e , m^* , ϵ_0 , e and N are the refractive index, the wavelength, the background permittivity, the plasma frequency, the relaxation time, the electron mobility, the electron mass, the electron effective mass, the vacuum permittivity, the electron

charge and the free carrier density, respectively. The free carrier density is approximately equal to the doping concentration in the heavily doped n-Si. In this case the doping concentration is equal to 10^{21}cm^{-3} [33].

Surface Plasmon-Polaritons (SPPs) are propagated between two gold layers. By applying a voltage between the two layers, a static electric field is created inside the dielectric layers. This field changes the refractive index of BaTiO₃, it also causes a shift in the real and imaginary parts of the n-Si refractive index. These variations also lead to alter the intensity of surface plasmon polaritons. To investigate these evolutions, it's necessary to obtain the dispersion relation.

2.2. Dispersion relation

In order to determine the dispersion relation for the structure in the on and off states, the TM mode solutions are used in the wave equation. By assuming that the time dependence part of the electromagnetic field is $e^{-i\omega t}$, the wave equation for the magnetic field component can be described by [34]:

$$\vec{\nabla} \times (\vec{\epsilon}^{-1} \vec{\nabla} \times \vec{H}) - \omega^2 \mu_0 \vec{H} = 0 \quad (6)$$

As it is required to stimulate the TM modes for SPP modes, the wave equation is given by [35]:

$$\frac{\partial^2 H_y}{\partial z^2} + \left(k_0^2 \epsilon_x - \beta^2 \frac{\epsilon_x}{\epsilon_z} \right) H_y = 0 \quad (7)$$

The components of the electric field for the TM modes are:

$$E_x = \frac{-i}{\omega \epsilon_0 \epsilon_x} \frac{\partial H_y}{\partial z} \quad (8)$$

$$E_z = \frac{-\beta}{\omega \epsilon_0 \epsilon_z} H_y \quad (9)$$

The n-Si layer is divided into 10 parts for the more accurate study of electrostatic and electrodynamic field effects. By assuming that the time and the x-coordinate dependent parts are in $e^{-i(\omega t - \beta x)}$ form, the solutions which satisfy equation (7) are:

$$H_y = \begin{cases} A_1 e^{ik_1(z-z_1)} & -\infty < z < z_1 \\ A_2 e^{ik_2(z-z_2)} + A_3 e^{-ik_2(z-z_2)} & z_1 < z < z_2 \\ A_4 e^{ik_3(z-z_3)} + A_5 e^{-ik_3(z-z_3)} & z_2 < z < z_3 \\ A_6 e^{ik_4(z-z_4)} + A_7 e^{-ik_4(z-z_4)} & z_3 < z < z_4 \\ \vdots & \vdots \\ A_{22} e^{ik_{12}(z-z_{12})} + A_{23} e^{-ik_{12}(z-z_{12})} & z_{12} < z < z_{13} \\ A_{24} e^{ik_{13}(z-z_{13})} + A_{25} e^{-ik_{13}(z-z_{13})} & z_{13} < z < z_{14} \\ A_{26} e^{ik_{14}(z-z_{14})} & z_{14} < z < +\infty \end{cases} \quad (10)$$

where $z_1 = 0$, $z_2 = h_{\text{Au}}$, $z_3 = h_{\text{Au}} + \frac{h_{\text{n-Si}}}{10}$, $z_4 = h_{\text{Au}} + \frac{2h_{\text{n-Si}}}{10}$, ..., $z_{12} = h_{\text{Au}} + \frac{10h_{\text{n-Si}}}{10}$, $z_{13} = h_{\text{Au}} + h_{\text{n-Si}} + h_{\text{BaTiO}_3}$, $z_{14} = h_{\text{Au}} + h_{\text{n-Si}} + h_{\text{BaTiO}_3}$. The components of the electric field of the TM mode can be obtained by inserting H_y , relation (10), into equations (8) and (9). In relation (10), k is the transverse propagation constant, which for all layers except the BaTiO₃ layer, is equal to:

$$k_m = \sqrt{\epsilon_m k_0^2 - \beta^2} \quad (11)$$

due to $\epsilon_x = \epsilon_z$, and for the BaTiO₃ layer is equal to [35]:

$$k_{13} = \sqrt{\epsilon_x k_0^2 - \beta^2 \frac{\epsilon_x}{\epsilon_z}} \quad (12)$$

where β is the propagation constant of SPP mode and ϵ_x and ϵ_z are the permittivities of the anisotropic layer in the x and z directions respectively also k_0 is the wavenumber in the free space. By applying the boundary conditions to H_y and E_z , one can obtain

$$M_{26 \times 26}(\lambda, \beta) \cdot A_{26 \times 1} = 0 \quad (13)$$

where λ is the vacuum wavelength and $A_{26 \times 1}$ is a column matrix that describes the constants in front of the exponential functions in relation (10).

In order to achieve the dispersion relation, the determinant of $M_{26 \times 26}$ should be zero [36]. The propagation constant, which it could be a complex number, is acquired by solving the dispersion relation per wavelength.

2.3. Solving method

Here, the Nelder-Mead method [37] is applied to solve the dispersion relation as this is an optimization method and it is not needed to take differentiation for finding the value of the parameters for minimizing the absolute value of the dispersion relation. The standard error to stop the numerical calculation is $\epsilon = 2.2204 \times 10^{-16}$. The absorption coefficient and the effective propagation length are respectively calculated as:

$$\alpha = 2\text{Im}[\beta] \quad (14)$$

and

$$L_e = \frac{1}{\alpha} \quad (15)$$

The 1dB on-off length can be defined as:

$$L_{1\text{dB}} = \frac{1}{(\log_{10} e) \Delta \alpha} \quad (16)$$

where $\Delta \alpha = |\alpha_{\text{off}} - \alpha_{\text{on}}|$ is the difference of the absorption coefficients in which α_{off} and α_{on} are the absorption coefficients of the off state and the on state, respectively. The extinction ratio,

$$E_R = (\log_{10} e) \Delta \alpha L, \quad (17)$$

is equal to 1dB in an arbitrary chosen DC voltage where L is the device length. At last, it is worthy to illustrate a parameter for comparing the efficiency of the presented absorption plasmonic modulator based on the above-defined quantities called the figure of merit (FoM) [36,38]:

$$\text{FoM} = \frac{L_e}{L_{1\text{dB}}} = (\log_{10} e) \frac{|\alpha_{\text{off}} - \alpha_{\text{on}}|}{\alpha_{\text{state}}} \quad (18)$$

where, α_{state} , is the residual absorption coefficient [38].

2.4. Applied static electric field

In general, the nonlinear Poisson equation is given by [39]:

$$\vec{\nabla} \cdot \vec{\epsilon}_s \vec{\nabla} \varphi = -\frac{\rho}{\epsilon_0} \quad (19)$$

for applying the static electric field in an anisotropic media. The charge density is zero ($\rho = 0$) for the BaTiO_3 layer. The nonlinear Poisson equation of this case is solved in one dimension. The electric potential at the interfaces can be acquired by the following boundary conditions:

$$\frac{U}{d} = \epsilon_{s,z} \frac{d\phi}{dz} \Big|_{z \rightarrow + (h_{Au} + h_{n-Si})} = \epsilon_{s,n-Si} \frac{d\phi}{dz} \Big|_{z \rightarrow - (h_{Au} + h_{n-Si})} \quad (20)$$

$$\phi(z) = 0 \quad \text{for } z \rightarrow +h_{Au} \quad (21)$$

and

$$\phi(z) = U \quad \text{for } z = h_{Au} + h_{n-Si} + h_{BaTiO_3} \quad (22)$$

where ϕ is the electrical potential, $\epsilon_{s,z}$ is the relative static permittivity of the BaTiO₃ in z-direction and $\epsilon_{s,n-Si}$ is the relative static permittivity of the n-Si.

For the n-Si layer, via exploiting the Thomas- Fermi screening theory [36], the Poisson equation can be rewritten as:

$$\nabla^2 \phi = \frac{e(N_i(z) - N_0)}{\epsilon_0 \epsilon_{s,n-Si}} \quad (23)$$

where

$$N_i(z) = \frac{1}{3\pi^2} \left(\frac{8\pi^2 m^*}{h^2} \right) (E_f + e\phi(z)) \quad (24)$$

$$\epsilon_{s,n-Si} = 11.688 + \frac{1.635 \times 10^{-19} N_D}{1 + 1.172 \times 10^{-21} N_D} \quad (25)$$

$$\epsilon_{s,z} = 135 \quad (29)$$

The Fermi energy, E_f , in equation (24) is defined as:

$$E_f = \left(\frac{h^2}{8\pi^2} \right) [3\pi^2 N_0]^{2/3} \quad (26)$$

where N_0 is the bulk free carrier density of the n-Si, N_D is the concentration of donors in the n-Si, m^* is the electron effective mass of the n-Si, E_f is the Fermi energy of the n-Si, h is the Planck constant, N_i is the free carrier density of the n-Si [36,40].

The finite difference method with the meshing number of 6000 is applied for solving equation (23) for the n-Si layer [41]. The effects of applying voltage on the refractive index of the n-Si layer can be studied by solving the Poisson equation in this layer where N_i is obtained in 10 parts of the n-Si layer and thus by substituting N_i in relation (3)

For the BaTiO₃ layer, the boundary conditions (20) and (22) are used to solve equation (27). Accordingly, the obtained static electric field induces an alteration in the ordinary and extraordinary refractive index which can be characterized by:

$$\frac{d^2 \phi}{dz^2} = 0 \quad (27)$$

$$\begin{bmatrix} \Delta \left(\frac{1}{n^2} \right)_1 \\ \Delta \left(\frac{1}{n^2} \right)_2 \\ \Delta \left(\frac{1}{n^2} \right)_3 \\ \Delta \left(\frac{1}{n^2} \right)_4 \\ \Delta \left(\frac{1}{n^2} \right)_5 \\ \Delta \left(\frac{1}{n^2} \right)_6 \end{bmatrix} = \begin{bmatrix} r_{11} & r_{12} & r_{13} \\ r_{21} & r_{22} & r_{23} \\ r_{31} & r_{32} & r_{33} \\ r_{41} & r_{42} & r_{43} \\ r_{51} & r_{52} & r_{53} \\ r_{61} & r_{62} & r_{63} \end{bmatrix} \begin{bmatrix} E_x \\ E_y \\ E_z \end{bmatrix} = \vec{r} \cdot \vec{E} \quad (28)$$

and

$$\vec{\eta} = [\frac{1}{n^2}] = \begin{bmatrix} \frac{1}{n_x^2} + \Delta(\frac{1}{n^2})_1 & \Delta(\frac{1}{n^2})_6 & \Delta(\frac{1}{n^2})_5 \\ \Delta(\frac{1}{n^2})_6 & \frac{1}{n_y^2} + \Delta(\frac{1}{n^2})_2 & \Delta(\frac{1}{n^2})_4 \\ \Delta(\frac{1}{n^2})_5 & \Delta(\frac{1}{n^2})_4 & \frac{1}{n_z^2} + \Delta(\frac{1}{n^2})_3 \end{bmatrix} \quad (29)$$

where $\vec{\eta}$ is the linear electro-optical coefficients matrix (Pockels) described in the standard crystallographic coordinate system that the z-direction indicates the crystal optical axis[42]. Here, $r_{13} = r_{23} = 19.5[\frac{\text{pm}}{\text{V}}]$, $r_{33} = 97[\frac{\text{pm}}{\text{V}}]$, $r_{42} = r_{51} = 1640[\frac{\text{pm}}{\text{V}}]$ and the other coefficients are zeroes [43]. $\vec{\eta}$ is the electro-optically perturbed impermeability tensor where $\Delta(\frac{1}{n^2})_m$ is the electro-optically induced variation of the impermeability tensor element, and n_x , n_y , and n_z are the refractive indices in x, y, and z-directions, respectively. The resulted refractive indices by applying the voltage are used for solving the dispersion relation in the off state.

3. Results and Analysis

3.2. Absorption Modulation

Regard to the variation of the imaginary part of the propagation constant of the proposed structure with the applied voltage, it can be utilized as an absorption modulator. The absorption coefficient of the modulator for the on and off states and its dependence to the thickness of the layer are shown in Fig. 2. According to fig. 2, it is understood that the absorption coefficient increases by applying the voltage and it is switched from the on state to the off state. By increasing the thickness of the n-Si layer the absorption coefficient of the on state has small changes with respect to the off state. Fig. 2 also indicates that the absorption coefficient of the on state increase by decreasing the thickness of the n-Si layer but this is not true for the off state. The maximum value of the absorption coefficient for the off state occurs at the 12nm thickness of the n-Si layer while it happens at the 10nm thickness for the on state.

The absorption coefficient of the on and off states increase by decreasing the thickness of the BaTiO₃ layer. In addition, by comparing the figs. 2(a), 2(b) and 2(c), it is found that the absorption coefficients of the both states decrease by increasing the thickness of the gold layer.

As high value of the figure of merit (FoM) is appreciated for the absorption modulators, it is necessary to increase the effective propagation length and decrease the 1dB on-off length. Fig. 3 shows the effective propagation length for different thicknesses of the n-Si, the BaTiO₃ and the gold layers in the on state. It is indicated that the effective propagation length gets larger by increasing the thicknesses of the layers. In fig. 4, it is shown that the thickness of the gold layer does not have a significant effect on the 1dB on-off length. But increasing the thickness of the BaTiO₃ layer change the 1dB on-off length inversely. Also, the minimum value of the 1dB on-off length occurred at a thickness of 15nm for the n-Si layer.

As mentioned earlier, the FoM parameter of the modulators depends on the effective propagation length and the 1dB on-off length. Here, one can discuss the FoM parameter of the presented modulator by the obtained results of fig. 4. The FoM of our modulator for different thicknesses is presented in fig. 5. Increasing the thicknesses of the gold and the BaTiO₃ layers result in growing the FoM parameter. The optimized configuration for the modulator is specified by the maximum value of the FoM parameter. The maximum value of the FoM is 12.79 which is obtained at an Air(∞)/Au(50nm)/BaTiO₃(30nm)/n-Si(13nm)/Au(50nm)/TSNAO(∞) multilayer configuration.

This value of FoM is much larger than the FoM of the previously reported device in ref. [36] which it expresses that our modulator has higher performance than the presented modulator in that reference as the effective propagation length and the 1dB on-off length have significant contributions on the performance of modulators. The origin of this value of FoM for our modulator is related to the high value of refractive index of BaTiO₃ which has an impact on transferring a large amount of energy to the n-Si layer. So, the refractive index of n-Si layer and consequently the absorption coefficient of the configuration change a lot. In addition, as the static permittivity of BaTiO₃ is high the electrical power for changing the refractive index of active materials will be reduced. Fig. 6(a) and fig. 6(b) show the propagation constant and the absorption coefficient for the optimized configuration in the on and the off states, respectively. The electric and the magnetic fields, as well as the time-averaged Poynting's vector for the optimized configuration in the on and the off states, are shown in fig. 7. Fig. 7(a)-7(d) shows that the structure has a good mode confinement in the structure moreover fig. 7(e) and fig. 7(f) indicate that the time-averaged Poynting's vector in the n-Si and the BaTiO₃ layers increase for the off state which it causes that the sensitivity of the modulator increases for changing the absorption coefficient in the active region.

4. Conclusion

In this study, an absorption plasmonic modulator is introduced and its operational parameters are numerically examined. It is noteworthy that for more realistic simulation, the Pockels effect at the BaTiO₃ and the free carrier dispersion effect at the n-type silicon are considered simultaneously. Here, the related parameters of the absorption modulation are investigated as a function of different thicknesses. The maximum value of the figure of merit, which occurs at an Air(∞)/Au(50nm)/BaTiO₃(30nm)/n-Si(12nm)/Au(50nm)/TSNAO(∞) multilayer structure, is equal to 12.79. Compared with the designed and fabricated plasmonic modulators [36,38,44,45,46], the FoM of our modulator is high which predicts higher performance with respect to them. By applying voltage, the energy flow increases in the n-Si and the barium titanate layers, hence, it causes that the plasmonic mode is more sensitive for changing the refractive indexes of these two layers. According to our results, the presented modulator is promising for exploiting as an intensity modulator, so it can be used in the plasmonic integrated circuits and due to compatibility with CMOS technology it can be integrated with microelectronic systems.

References

- [1] G.E. Moore, Progress in digital integrated electronics [Technical literature, copyright 1975 IEEE. reprinted, with permission. technical digest. international electron devices meeting, IEEE, 1975, pp. 11-13.], IEEE Solid-State Circuits Soc. Newsl. 20 (2006).
- [2] R. Zia, J.A. Schuller, A. Chandran, M.L. Brongersma, Plasmonics: the next chip-scale technology, Mater. Today. 9 (2006) 20–27.
- [3] Gramotnev, Dmitri K, and Sergey I Bozhevolnyi, 'Plasmonics beyond the Diffraction Limit', Nature Photonics, 4 (2010), 83.
- [4] J. Leuthold, C. Hoessbacher, S. Muehlbrandt, A. Melikyan, M. Kohl, C. Koos, W. Freude, V. Dolores-Calzadilla, M. Smit, I. Suarez, Plasmonic communications: light on a wire, Opt. Photonics News. 24 (2013) 28–35.

- [5] A. Melikyan, L. Alloatti, A. Muslija, D. Hillerkuss, P.C. Schindler, J. Li, R. Palmer, D. Korn, S. Muehlbrandt, D. Van Thourhout, High-speed plasmonic phase modulators, *Nat. Photonics*. 8 (2014) 229.
- [6] J.A. Dionne, K. Diest, L.A. Sweatlock, H.A. Atwater, PlasMOSor: a metal– oxide– Si field effect plasmonic modulator, *Nano Lett.* 9 (2009) 897–902.
- [7] C. Haffner, W. Heni, Y. Fedoryshyn, D.L. Elder, A. Melikyan, B. Baeuerle, J. Niegemann, A. Emboras, A. Josten, F. Ducry, High-speed plasmonic Mach-Zehnder modulator in a waveguide, in: *Opt. Commun. (ECOC)*, 2014 Eur. Conf., IEEE, 2014: pp. 1–3.
- [8] W. Cai, J.S. White, M.L. Brongersma, Compact, high-speed and power-efficient electrooptic plasmonic modulators, *Nano Lett.* 9 (2009) 4403–4411.
- [9] G. Gagnon, N. Lahoud, G.A. Mattiussi, P. Berini, Thermally activated variable attenuation of long-range surface plasmon-polariton waves, *J. Light. Technol.* 24 (2006) 4391–4402.
- [10] J. Gosciniaik, S.I. Bozhevolnyi, T.B. Andersen, V.S. Volkov, J. Kjelstrup-Hansen, L. Markey, A. Dereux, Thermo-optic control of dielectric-loaded plasmonic waveguide components, *Opt. Express*. 18 (2010) 1207–1216.
- [11] Z. Qi, G. Hu, B. Yun, X. Zhang, Y. Cui, Fast response and low power consumption 1×2 thermo-optic switch based on dielectric-loaded surface plasmon polariton waveguides, *J. Mod. Opt.* 63 (2016) 1354–1363.
- [12] S. Zhu, G.Q. Lo, D.L. Kwong, Electro-absorption modulation in horizontal metal-insulator-silicon-insulator-metal nanoplasmonic slot waveguides, *Appl. Phys. Lett.* 99 (2011) 151114.
- [13] U. Koch, C. Hössbacher, J. Niegemann, C. Hafner, J. Leuthold, Digital plasmonic absorption modulator exploiting epsilon-near-zero in transparent conducting oxides, *IEEE Photon. J.* 8 (2016).
- [14] S. Randhawa, S. Lachèze, J. Renger, A. Bouhelier, R.E. de Lamaestre, A. Dereux, R. Quidant, Performance of electro-optical plasmonic ring resonators at telecom wavelengths, *Opt. Express*. 20 (2012) 2354–2362.
- [15] A. Melikyan, L. Alloatti, A. Muslija, D. Hillerkuss, P.C. Schindler, J. Li, R. Palmer, D. Korn, S. Muehlbrandt, D. Van Thourhout, High-speed plasmonic phase modulators, *Nat. Photonics*. 8 (2014) 229.
- [16] C. Hössbacher, A. Josten, B. Baeuerle, Y. Fedoryshyn, H. Hettrich, Y. Salamin, W. Heni, C. Haffner, C. Kaiser, R. Schmid, Plasmonic modulator with > 170 GHz bandwidth demonstrated at 100 GBd NRZ, *Opt. Express*. 25 (2017) 1762–1768.
- [17] A. Joushaghani, B.A. Kruger, S. Paradis, D. Alain, J. Stewart Aitchison, J.K.S. Poon, Sub-volt broadband hybrid plasmonic-vanadium dioxide switches, *Appl. Phys. Lett.* 102 (2013) 61101.
- [18] J.T. Kim, CMOS-compatible hybrid plasmonic modulator based on vanadium dioxide insulator-metal phase transition, *Opt. Lett.* 39 (2014) 3997–4000.

- [19] S.-J. Kim, H. Yun, K. Park, J. Hong, J.-G. Yun, K. Lee, J. Kim, S.J. Jeong, S.-E. Mun, J. Sung, Active directional switching of surface plasmon polaritons using a phase transition material, *Sci. Rep.* 7 (2017) 43723.
- [20] A. Emboras, I. Goykhman, B. Desiatov, N. Mazurski, L. Stern, J. Shappir, U. Levy, Nanoscale plasmonic memristor with optical readout functionality, *Nano Lett.* 13 (2013) 6151–6155.
- [21] U. Koch, C. Hoessbacher, A. Emboras, J. Leuthold, Optical memristive switches, *J. Electroceramics.* 39 (2017) 239–250.
- [22] S.I. Bozhevolnyi, V.S. Volkov, E. Devaux, J.-Y. Laluet, T.W. Ebbesen, Channel plasmon subwavelength waveguide components including interferometers and ring resonators, *Nature.* 440 (2006) 508.
- [23] J.A. Dionne, H.J. Lezec, H.A. Atwater, Highly confined photon transport in subwavelength metallic slot waveguides, *Nano Lett.* 6 (2006) 1928–1932.
- [24] K.-Y. Jung, F.L. Teixeira, R.M. Reano, Surface plasmon coplanar waveguides: Mode characteristics and mode conversion losses, *IEEE Photon. Technol. Lett.* 21 (2009) 630–632.
- [25] E. Verhagen, M. Spasenović, A. Polman, L.K. Kuipers, Nanowire plasmon excitation by adiabatic mode transformation, *Phys. Rev. Lett.* 102 (2009) 203904.
- [26] A. V Krasavin, A. V Zayats, Silicon-based plasmonic waveguides, *Opt. Express.* 18 (2010) 11791–11799.
- [27] C. Ye, S. Khan, Z.R. Li, E. Simsek, V.J. Sorger, λ -size ITO and graphene-based electro-optic modulators on SOI, *IEEE J. Sel. Top. Quantum Electron.* 20 (2014) 40–49.
- [28] J.A. Dionne, L.A. Sweatlock, M.T. Sheldon, A.P. Alivisatos, H.A. Atwater, Silicon-based plasmonics for on-chip photonics, *IEEE J. Sel. Top. Quantum Electron.* 16 (2010) 295–306.
- [29] X.A. Zhang, A. Bagal, E.C. Dandley, J. Zhao, C.J. Oldham, B. Wu, G.N. Parsons, C. Chang, Ordered 3D Thin-Shell Nanolattice Materials with Near-Unity Refractive Indices, *Adv. Funct. Mater.* 25 (2015) 6644–6649.
- [30] P.G. Etchegoin, E.C. Le Ru, M. Meyer, An analytic model for the optical properties of gold, *J. Chem. Phys.* 125 (2006) 164705.
- [31] R. Soref, R.E. Peale, W. Buchwald, Longwave plasmonics on doped silicon and silicides, *Opt. Express.* 16 (2008) 6507–6514.
- [32] S.D. Setzler, P.G. Schunemann, T.M. Pollak, L.A. Pomeranz, M.J. Missey, D.E. Zelmon, Periodically Poled Barium Titanate as a New Nonlinear Optical Material, in: *Adv. Solid State Lasers*, Optical Society of America, 1999: p. MD1.
- [33] B.G. Streetman, S.K. Banerjee, *Solid State Electronic Devices: Global Edition*, Pearson education, 2016.
- [34] A.B. Fallahkhair, K.S. Li, T.E. Murphy, Vector finite difference modesolver for anisotropic dielectric waveguides, *J. Light. Technol.* 26 (2008) 1423–1431.

- [35] A. Kumar, S.F. Yu, X. Li, Design and analysis of a surface plasmon polariton modulator using the electro-optic effect, *Appl. Opt.* 48 (2009) 6600–6605.
- [36] A. Melikyan, N. Lindenmann, S. Walheim, P.M. Leufke, S. Ulrich, J. Ye, P. Vincze, H. Hahn, T. Schimmel, C. Koos, Surface plasmon polariton absorption modulator, *Opt. Express*. 19 (2011) 8855–8869.
- [37] J.C. Lagarias, J.A. Reeds, M.H. Wright, P.E. Wright, Convergence properties of the Nelder-Mead simplex method in low dimensions, *SIAM J. Optim.* 9 (1998) 112–147.
- [38] V.E. Babicheva, A. V Lavrinenko, Plasmonic modulator optimized by patterning of active layer and tuning permittivity, *Opt. Commun.* 285 (2012) 5500–5507.
- [39] L. Hu, G.-W. Wei, Nonlinear Poisson equation for heterogeneous media, *Biophys. J.* 103 (2012) 758–766.
- [40] S. Ristić, A. Prijić, Z. Prijić, Dependence of static dielectric constant of silicon on resistivity at room temperature, *Serbian J. Electr. Eng.* 1 (2004) 237–247.
- [41] J. Kierzenka, L.F. Shampine, A BVP solver based on residual control and the Matlab PSE, *ACM Trans. Math. Softw.* 27 (2001) 299–316.
- [42] M. Bass, E.W. Van Stryland, D.R. Williams, W.L. Wolfe, *Handbook of Optics Volume II Devices, Measurements, Handb. Opt. Vol. II Devices, Meas. Prop.* 2nd Ed. by Michael Bass, Eric W. Van Stryland, David R. Williams, William L. Wolfe New York, NY McGraw-Hill, INC, 1995. (1995).
- [43] R.W. Boyd, *Nonlinear optics*, Elsevier, 2003.
- [44] A. V Krasavin, A. V Zayats, Photonic signal processing on electronic scales: electro-optical field-effect nanoplasmonic modulator, *Phys. Rev. Lett.* 109 (2012) 53901.
- [45] A.P. Vasudev, J.-H. Kang, J. Park, X. Liu, M.L. Brongersma, Electro-optical modulation of a silicon waveguide with an “epsilon-near-zero” material, *Opt. Express*. 21 (2013) 26387–26397.
- [46] S. Zhu, G.Q. Lo, D.L. Kwong, Design of an ultra-compact electro-absorption modulator comprised of a deposited TiN/HfO₂/ITO/Cu stack for CMOS backend integration, *Opt. Express*. 22 (2014) 17930–17947.

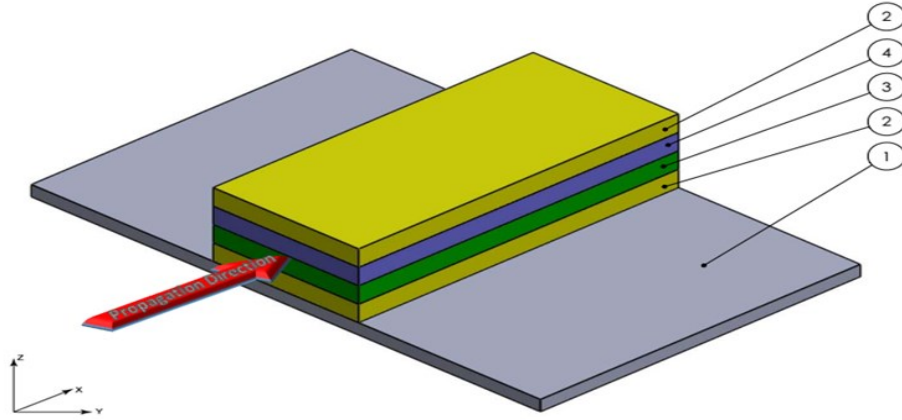


Figure 1. Schematic structure of designed modulator; (1) thin-shell nanolattice Al_2O_3 with near unity refractive index substrate (2) gold layer (3) n-Si layer (4) BaTiO_3 layer.

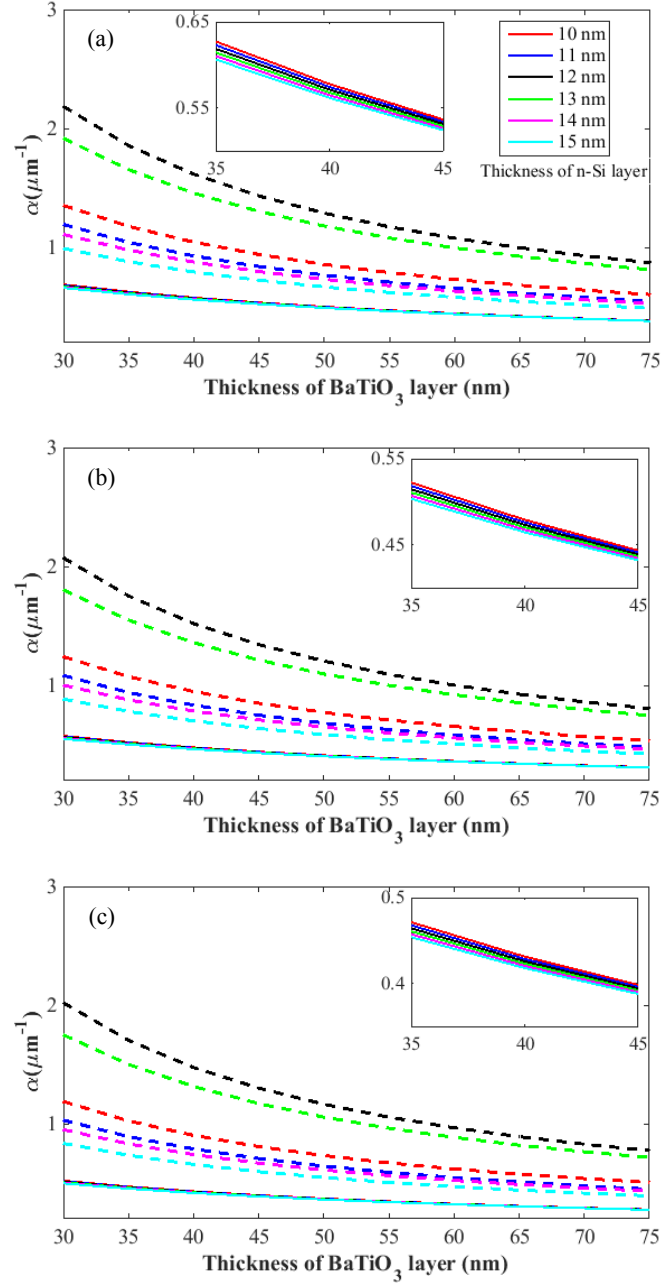


Fig. 2. Absorption coefficient of the structure for different thicknesses of the BaTiO_3 and the n-Si layers at 30nm (a), 40nm (b) and 50nm (c) thickness of gold layer for on (solid line) and off (dashed line) states. Each color indicates different thickness of the n-Si layer which specified in the fig. 2(a) as inset.

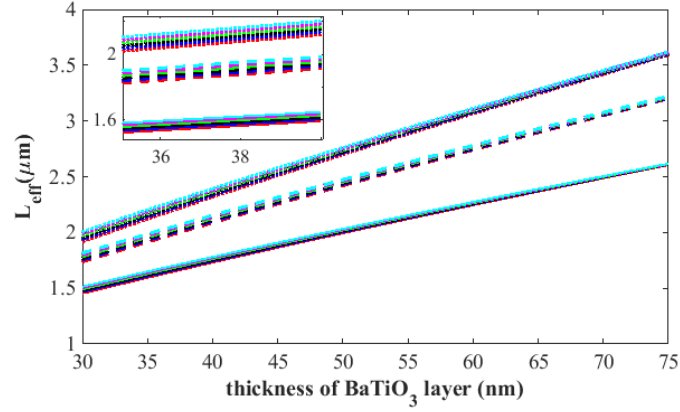


Fig. 3. Effective propagation length of the structure for different thicknesses of the BaTiO₃ and the n-Si layers at 30nm (solid line), 40nm (dashed line) and 50nm (dotted line) thickness of the gold layer. Colors represent the same thicknesses of the n-Si layers as fig. 2.

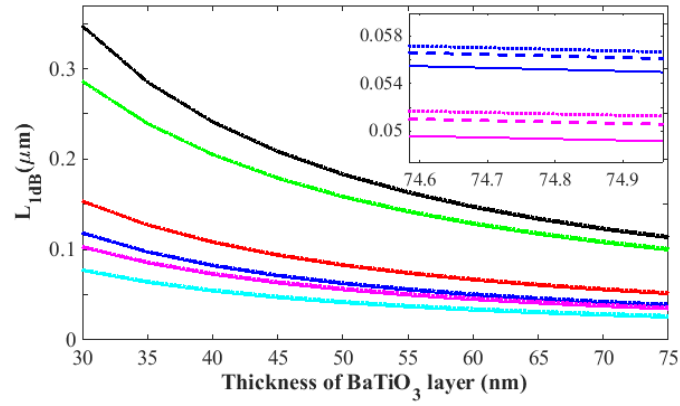


Fig. 4. 1dB on-off length of the structure is plotted for different thicknesses of the BaTiO₃ and n-Si layers at 30nm (solid line), 40nm (dashed line) and 50nm (dotted line) thickness of the gold layer. Colors represent the same thicknesses of the n-Si layers as fig. 2.

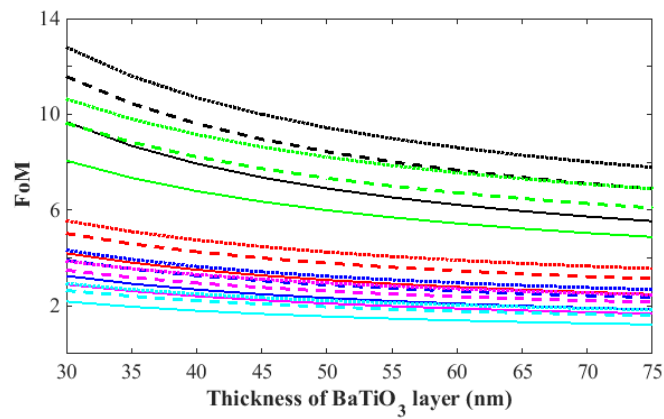


Fig. 5. Figure of merit (FoM) of the structure for different thicknesses of the BaTiO₃ and the n-Si layers at 30nm (solid line), 40nm (dashed line) and 50nm (dotted line) thickness of the gold layer. Colors represent the same thicknesses of the n-Si layers as fig. 2.

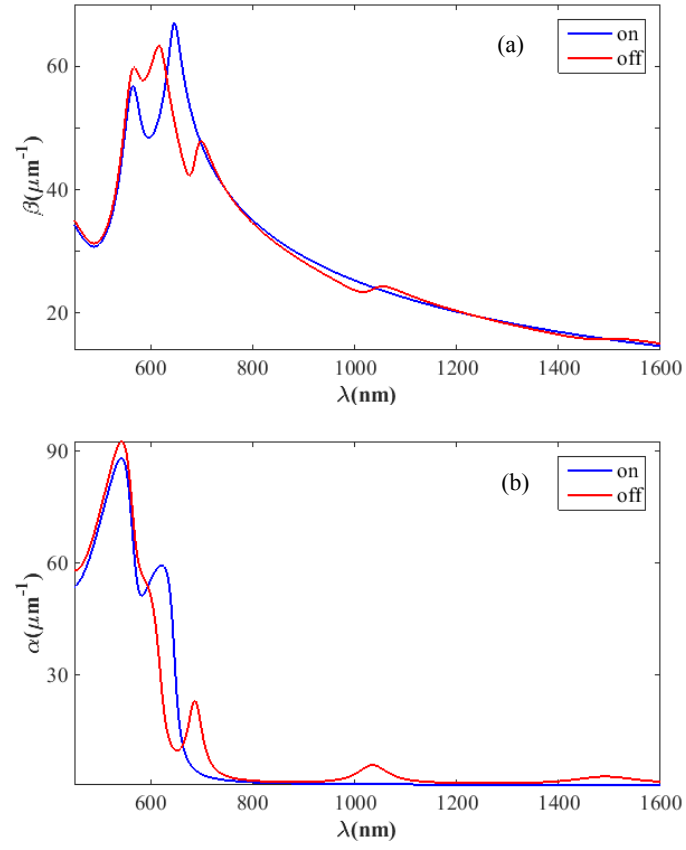


Fig 6. The propagation constant (a) and absorption coefficient (b) of the optimized modulator for the off (red line) and the on (blue line) states.

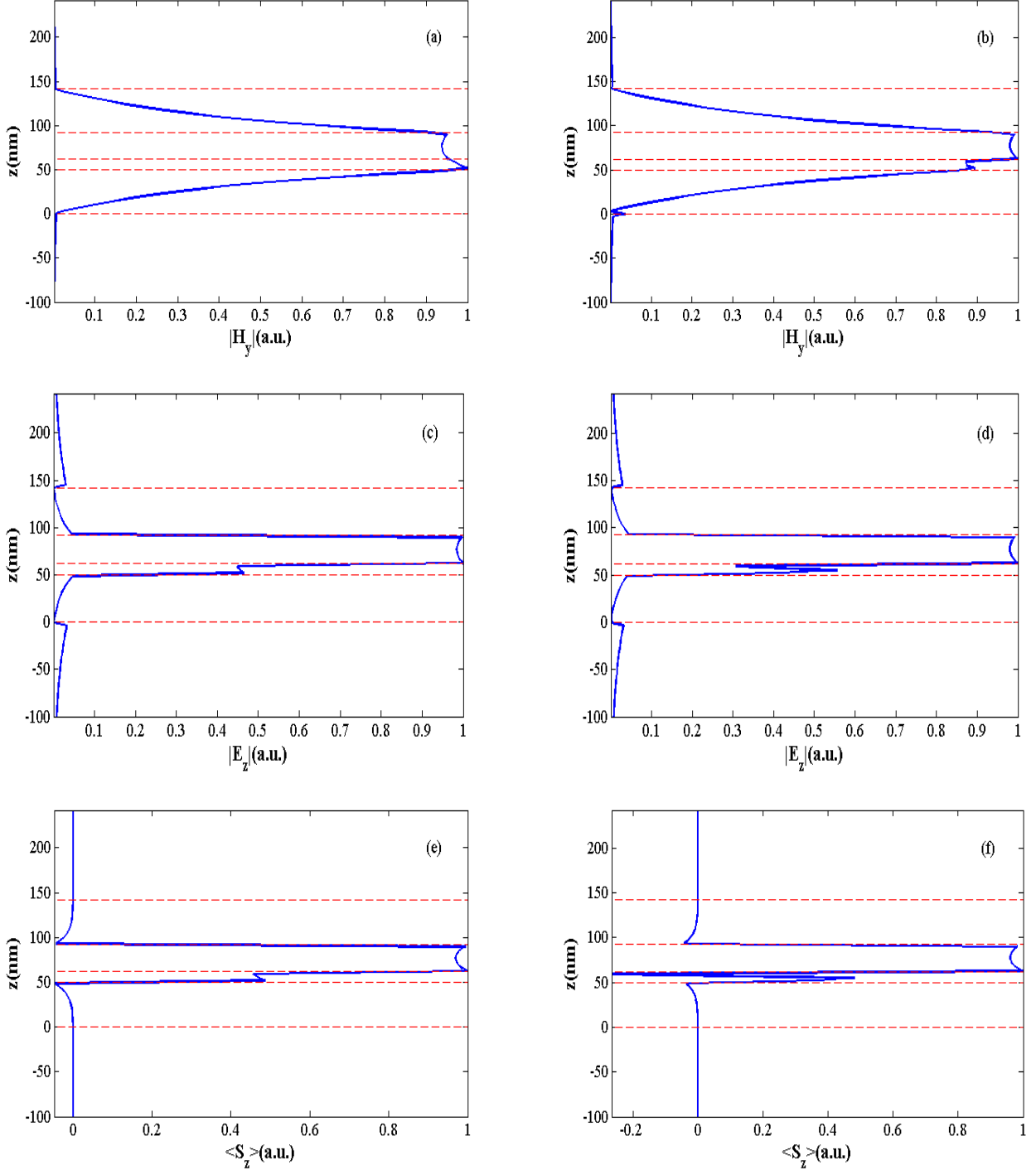


Fig. 7. The normalized magnetic field (a), z-component of the normalized electric field (c) and the normalized time-averaged Poynting's vector (e) of the optimized modulator are plotted for the on state at 1.55 micrometer while (b), (d) and (f) indicate the same parameters as (a), (c) and (e) but for the off state.